

**Anatomical and pathophysiological profiles of cerebrocortical
responses to stimulating peripheral organs
innervated by the maxillary nerve**

Manabu Zama

Nihon University Graduate School of Dentistry

Major in Oral and Maxillofacial Surgery

(Directors: Profs. Morio Tonogi and Masayuki Kobayashi)

Index

Aim and Scope	-----	2
Abbreviations	-----	3
CHAPTER 1		
Introduction	-----	4
Materials and Methods	-----	5
Results	-----	7
Discussion	-----	13
CHAPTER 2		
Introduction	-----	16
Materials and Methods	-----	17
Results	-----	20
Discussion	-----	24
Conclusions	-----	28
Acknowledgements	-----	28
References	-----	29

This thesis is based on the following two articles:

- 1) Somatotopic organization and temporal characteristics of cerebrocortical excitation in response to nasal mucosa stimulation with and without an odor in the rat: an optical imaging study.
Zama M, Hara Y, Fujita S, Kaneko T, Kobayashi M.
Neuroscience. 377: 77-86, 2018.
- 2) Preceding administration of minocycline suppresses neuroplastic changes in cortical excitatory propagation in the model rat with partial infraorbital nerve ligation.
Zama M, Fujita S, Nakaya Y, Tonogi M, Kobayashi M.
Frontiers in Neurology. in press, 2019.

Aim and Scope

Orofacial sensations such as touch, pressure, temperature, and nociception are derived from the orofacial structures innervated by the trigeminal nerve, and play a critical role in regulating mastication, speech, swallowing, and protective reaction against noxious inputs. The maxillary nerve, a branch of the trigeminal nerve, innervates the middle part of face, nasal, and upper oral structures, a part of which are trigger points of abnormal pain. However, not a few basic mechanisms of their somatosensory information processing in the higher brain, the cerebral cortex, have remained unknown.

One of critical unsolved questions is how the mucosa sensation is organized in the somatosensory cortex. The map of the nasal mucosa and the effect of odors on their activities are largely unknown, though the somatosensory map of the face in the primary (S1) and secondary somatosensory cortices (S2) is clearly documented. Therefore, I first aimed to identify the cortical regions in S1 in response to air puff stimulation of the nasal mucosa using an optical imaging technique. Nasal mucosa stimulation excited the contralateral S1 and subsequently, the excitation spread toward the rostrally or ventrally adjacent sites. Upper pharynx stimulation initially activated this rostrally expanded site and the ventrally expanded region was likely to represent S2. The amplitude of S1 excitation was similar between air puff stimulation with and without an odor, amyl acetate. These results suggest that somatosensory information from the nasal mucosa and upper pharynx are processed in spatially continuous regions of S1, and interaction between somatosensory and olfactory systems is relatively small in contralateral S1.

Another issue that is desired to be clarified is the mechanisms of trigeminal neuropathic pain. Although recent studies have revealed the molecular mechanisms regarding chronic pain, estimation of the effectiveness of the pharmacological treatment has not been well provided especially in the central nervous system so far. The partial ligation of the infraorbital nerve (pl-ION), a branch of the maxillary nerve, is a superb method to mimic chronic trigeminal neuropathic pain and behavioral abnormality. Therefore, in the second part of this study, I examined whether pl-ION induces neuroplastic changes in the cerebral cortex and investigated effects of minocycline on the cortical neuroplastic changes. Electrical stimulation to the whisker pad skin induced smaller excitation in S1 of 3 d after pl-ION in comparison to that in the sham. In contrast, cerebral cortical responses to the mandibular molar dental pulp and mentum skin stimuli increased both in S1, and S2 and insular oral region (S2/IOR) after pl-ION. Administration of minocycline from 1 d before to 2 d after pl-ION partially recovered the pl-ION-induced changes in S1 and S2/IOR 3 days after pl-ION. These results suggest that somatosensory and insular cortical excitation is changed by pl-ION, and the preceding injection of minocycline counteracts the neuroplastic changes in the cortical activities.

These findings contribute to understand basic mechanisms of orofacial somatosensation in the cerebral cortex, which promotes to develop a new pharmacotherapy for trigeminal abnormal pain.

Abbreviations

3d-pl-ION: 3 d after pl-ION

3d-Sham: 3 d after sham operation

cMCA: caudal branch of the MCA

F: initial intensity of fluorescence

ΔF : change in the intensity of fluorescence

HWT: head-withdrawal threshold

IC: insular cortex

ION: infraorbital nerve

MCA: middle cerebral artery

pl-ION: partial ligation of ION

rMCA: rostral branch of the MCA

ROI: region of interest

S1: primary somatosensory cortex

S2: secondary somatosensory cortex

S2/IOR: S2 and IC related to the sensation in the oral structures

Vc: trigeminal spinal subnucleus caudalis

Chapter 1

Somatotopic organization and temporal characteristics of cerebrocortical excitation in response to nasal mucosa stimulation with and without an odor in the rat

Introduction

The nasal cavity composes a part of the air way and is anatomically located between the outside environment and the upper pharynx. Moreover, the nasal cavity receives and conveys both olfactory and somatosensory sensation to the central nervous system via the olfactory nerve (Sato et al., 2008) and the ophthalmic and maxillary divisions of the trigeminal nerve, respectively (Tsubone, 1989; Sant'Ambrogio et al., 1995; Brand, 2006). Olfactory information processing in the central nervous system has been extensively explored and chemotopy has been demonstrated in the olfactory bulb (Johnson and Leon, 2007). In addition, recent studies have revealed representations of odor in the piriform cortex (Rennaker et al., 2007; Stettler and Axel, 2009). On the other hand, somatosensory information from the nasal mucosa and skin could be processed in the somatosensory cortex in a similar fashion because both the outer and inner nose are innervated by branches of the trigeminal nerve. Recently, fMRI study in humans indicated that tactile information from the nasal mucosa is processed in the somatosensory cortex close to regions that process information from the alar wing of the nose and the hand (Gastl et al., 2014). This finding raises the possibility that information from the nasal mucosa of rats is similarly processed in the somatosensory area adjacent to the region that processes information from the outer nose.

The trigeminal nerve innervates the nasal cavity and responds to cold, pressure, and some chemical substances (Anton and Peppel, 1991; Sant'Ambrogio et al., 1995), whereas, the ethmoidal nerve in rats is activated by air flow at room or low temperature but is suppressed by high temperature (Tsubone, 1989). A large proportion of afferents that respond to air flow are also responsive to tactile stimuli. The ethmoidal nerve also responds to pressure and the fibers connect mostly to negative pressure receptors (Tsubone, 1990). These neural activities might influence the processing of olfactory information in the higher brain, especially the cerebral cortex, because somatosensory and olfactory information are processed simultaneously. Indeed, the trigeminal system plays a critical role in the lateralization of odors in humans (Croy et al., 2014). However, little is known regarding how somatosensory stimuli in the nasal mucosa with and without an odor activate the somatosensory cortex.

An *in vivo* optical imaging using a voltage-sensitive dye enables us to visualize not only the spatial pattern of cortical excitation but also the temporal features of cortical activation

with high resolution (Kobayashi et al., 2010; Horinuki et al., 2015, 2016; Nakamura et al., 2015, 2016; Fujita et al., 2017; Kaneko et al., 2017; Kobayashi and Horinuki, 2017). In this regard, by using this technique, I elucidated the cortical responses that processes somatosensory information from the nasal mucosa to address: (1) whether neural activity induced by somatosensory stimulation of the nasal mucosa in rats is located adjacent to the region corresponding to the nasal tip and upper pharynx, and (2) whether activities of the contralateral primary somatosensory cortex (S1) is influenced by an odor.

Materials and Methods

The Animal Experimentation Committee of Nihon University approved the experiments, and all experiments were performed according to the institutional guidelines for the care and use of experimental animals described in the National Institutes of Health Guide for the Care and Use of Laboratory Animals. All efforts were made to minimize animal suffering and to reduce the number of animals used.

Animals and surgical procedures for in vivo optical imaging

Eight-week-old male Sprague-Dawley rats (Sankyo Laboratories, Tokyo, Japan) weighing 225.0 ± 8.7 g (mean \pm SEM; $n = 33$) were used for optical imaging experiments. The rats were housed in cages ($27 \times 45 \times 20$ cm) in an animal room where temperature ($23 \pm 2^\circ\text{C}$) and humidity ($55 \pm 5\%$) were controlled with a 12 h light/dark cycle (lights on at 0700 h; off at 1900 h). Food and water were freely available for approximately 1 week until the experimental day. Optical imaging using a voltage-sensitive dye (RH-1691, Optical Imaging, New York, NY, USA) was performed as previously described (Kobayashi et al., 2010; Fujita et al., 2012, 2016, 2017; Horinuki et al., 2015, 2016; Nakamura et al., 2015, 2016). Briefly, the rats received an atropine methyl bromide injection (5 mg/kg, i.p.) and were anesthetized with urethane (1.5 g/kg, i.p., Sigma-Aldrich, St. Louis, MO, USA). Anesthesia efficacy was gauged by the toe pinch reflex, and additional urethane was administered as needed. Body temperature was monitored using a rectal probe and was maintained at approximately 37°C using a heating pad (BWT-100, Bio Research Center, Osaka, Japan). Rats were fixed to a custom-made stereotaxic snout frame, which was tilted 60° laterally for imaging the surface of the left ventral part of the S1 using a CCD camera (MiCAM02, Brainvision, Tokyo, Japan). Left temporal muscle and zygomatic arch were carefully removed and a craniotomy was performed to expose S1 and the surrounding cortices, including the secondary somatosensory (S2), insular, and piriform cortices.

RH-1691 (1 mg/ml) in 0.9% saline was applied to the cortical surface for 1 h. RH-1691 fluorescence intensities were measured using the CCD camera system described above which was mounted on a stereomicroscope (Leica Microsystems, Wetzlar, Germany). Cortical surface was illuminated through a 632-nm excitation filter and a dichroic mirror using a tungsten-halogen lamp (CLS150XD, Leica Microsystems). Fluorescent emission was

captured through an absorption filter ($\lambda > 650$ -nm longpass, Andover, Salem, MA, USA). CCD camera had a $6.4 \times 4.8 \text{ mm}^2$ imaging area (184×124 pixels).

To remove signals that were due to acute bleaching of the dye, values in the absence of any stimuli were subtracted from each recording. Thus, each image was constructed from paired recordings with and without stimulation. Sampling rate was set at 250 Hz and the acquisition time was 1000 ms. Twenty-four consecutive images in response to the stimuli were averaged to reduce the noise described above.

Air puff stimulation

To apply somatosensory stimuli to the nasal mucosa and upper pharynx, a polyethylene tube (inner diameter = 0.5 mm) was inserted into the right nostril 1 mm and approximately 31 mm from the tip of the nose. The tube tip was set 1 mm away from the nose tip and tongue to stimulate the nasal skin and tongue, respectively. Air temperature was kept at room temperature (20-25°C). Air pressure range was 5-25 psi. Cortical responses to the air puff (100 ms) in the nasal mucosa were recorded from the left S1 and S2 by using *in vivo* optical imaging with a voltage-sensitive dye as mentioned above. In the case of imaging of the piriform cortex, the left nasal mucosa was stimulated.

Amyl acetate was used for odor stimulation. Briefly, amyl acetate (2 ml) solved in the mineral oil (8 ml) was filled in the glass bottle with a total volume of 100 ml. Continuous odorant stream (400 ml/min) was applied into the bottle and the outlet tube was connected to the Y-shaped tube whose tips were connected to the exhaust tube and the tube inserted into the nostril. These tubes were interconnected with the electromagnetic switching valves to switch the way of odor flow. Air was deodorized by passing two bottles filled with activated carbon. Vapor was ejected with the deodorized air (10-15 psi) to stimulate the nasal mucosa with amyl acetate.

Anatomy

After optical imaging, the regions responding to nasal mucosa and tip stimulation were marked by penetration with a needle. Subsequently, rats were deeply anesthetized with 5.0% isoflurane and perfused through the ascending aorta with saline, followed by 300 ml of a fixative containing 4% paraformaldehyde in 0.1 M phosphate buffer (pH = 7.4). Brains were removed, post-fixed overnight and cryoprotected in 30% sucrose with 0.1 M phosphate buffer. Brains were frozen, sectioned coronally at 50 μm , and stained with 0.25% thionine to examine the responding sites.

Data analysis

Optical imaging data were processed and analyzed using Brain Vision Analyzer software (Brainvision). Changes in the intensity of fluorescence (ΔF) of each pixel relative to the initial intensity of fluorescence (F) were calculated ($\Delta F/F$), and the ratio was processed with a spatial filter (9×9 pixels). A significant response was defined as a signal exceeding two times

the SD of the whole recording period. To compare initial responses of the nasal mucosa, nasal tip, upper pharynx, and tongue stimulation, grafted images were aligned across multiple rats using the rhinal fissure and MCA as landmarks. Locations of the initial responses were marked at the center position in the first frame that exhibited a significant increase in the optical signal. In this study, the responses showed dull but not sharp peaks (Figs. 1, 3). To evaluate activated areas and temporal profiles, I used the frames in which the optical signal exceeded 95% of the maximum amplitude in the center of the initial response. I defined the latency as the time elapsed between the onset of stimulation and the time at which a significant optical response was first detected. The peak amplitude was the maximum amplitude of an optical response at the point of the initial response. Time to peak was defined as the duration from the onset of stimulation to the frame in which the optical signal first exceeded 95% of the maximum amplitude. Rise time was defined as the duration from 20% - 80% of the maximum optical response, whereas, the decay time was defined as the duration from 80% - 20% of the maximum optical response. Half duration was considered the duration at half the maximum optical response.

Binomial test was performed using Excel (ver. 2010, Microsoft, Redmond, WA, USA). SigmaStat software (ver. 4.0, Systat Software, San Jose, CA, USA) was used for other statistical analyses and $p < 0.05$ was considered significant. All data were expressed as the means \pm SEM.

Results

Activation of the somatosensory cortex by air puff stimulation to the nasal mucosa and skin

A typical example of a response to air puff (20 psi) of the nasal mucosa is shown in Fig. 1A. In the ventral part of S1 and S2, the middle cerebral artery (MCA) generally ramifies into the rostral (rMCA, black arrow) and caudal branches (cMCA, white arrow). First neural excitation was elicited at the caudal site of the cMCA (Fig. 1A, black circle, white arrowhead "a"). Subsequently, the neural excitation spread rostrally (Fig. 1A, red circle, white arrowhead "b") and ventrally (Fig. 1A, blue circle, black arrowhead). A similar large response with a short delay was observed in the rostral region (Fig. 1C, red circle), whereas, a smaller excitation amplitude was observed in the ventral region (blue circle).

Optical responses to air puff stimulation were induced with a delay and abrupt increase in the amplitude (Fig. 1A, C). After reaching the plateau, signals decayed toward the baseline, even while air puff stimulation was applied. At the termination of stimulation, notches were occasionally observed (also see Fig. 3B).

To explore the spatial distribution patterns of the nasal mucosa- and skin-responding regions, the air puff stimulus was applied to the nasal tip in the same way as the nasal mucosa, except for the location of stimulation. Similar to the responses observed with nasal mucosa stimulation, neural excitation initially appeared in the somatosensory area rostral to the cMCA (Fig. 1B, white arrowhead "c"). Subsequently, faint excitation propagated toward the rostral

region (Fig. 1B, black arrowhead). Response to nasal mucosa stimulation was found in the rostral region in comparison to the response to nasal tip stimulation (Fig. 1A, B).

Regions initially activated by nasal mucosa and tip stimulation, as well as the rostral region that was subsequently activated by nasal mucosa stimulation, were lesioned in order to examine their precise location in Nissl sections (Fig. 1D, E; Paxinos and Watson, 2007). All lesions were located in S1, wherein, the granule cell layer (layer IV) was observed. The regions ventral to lesions involved a smaller amount of layer IV which suggests that they were located in S2.

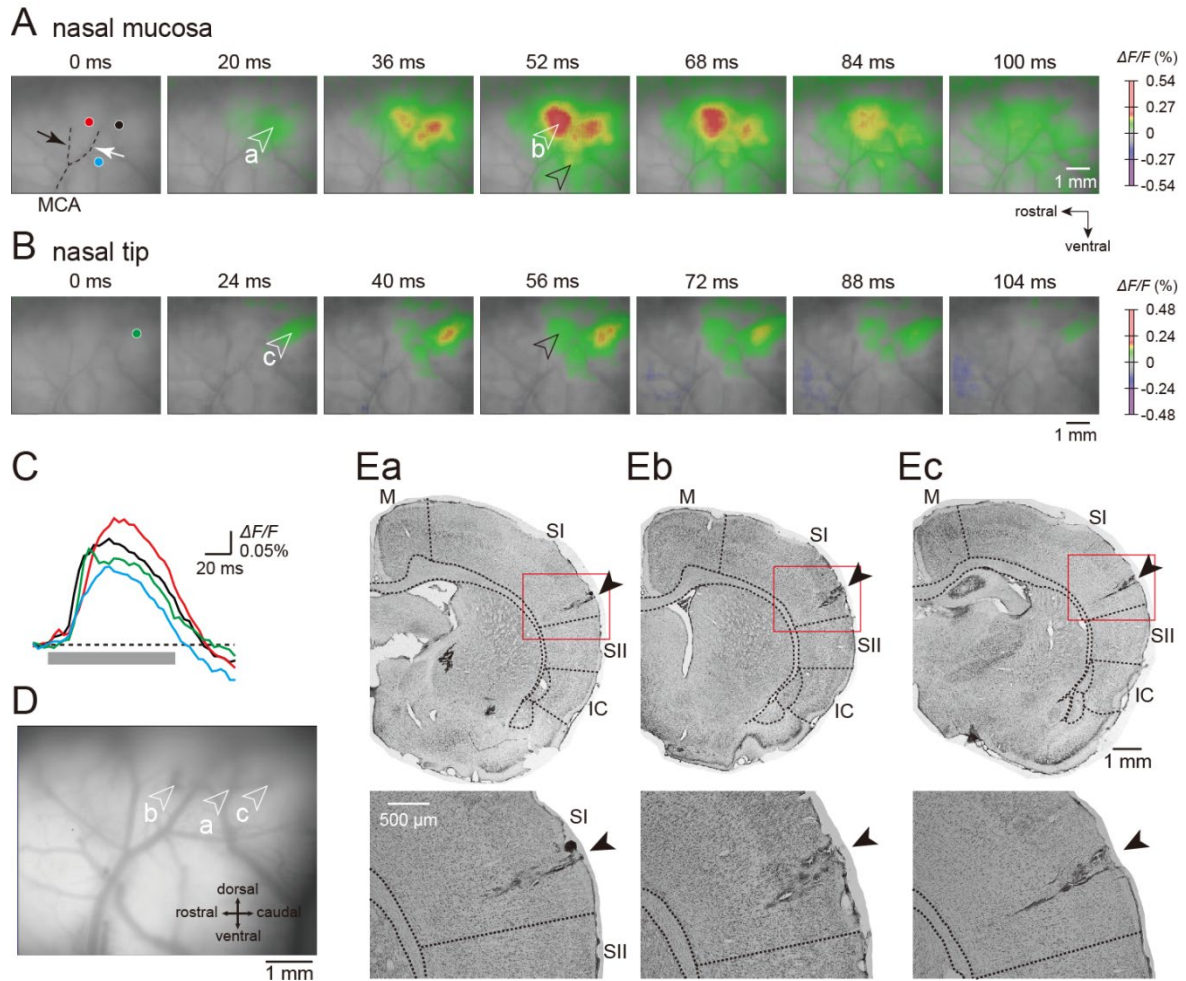


Figure 1. Responses to air puff application to the nasal mucosa and tip. (A) An example of excitatory propagation elicited by air puff stimulation (100 ms; 20 psi) of the nasal mucosa. Amplitude of optical signal ($\Delta F/F$) is color-coded and the time from the onset of air puff stimulation is shown at the top of each panel. Black and white arrows indicate the rostral and caudal branches, respectively, of the middle cerebral artery (MCA; broken line). Note that the first excitation was elicited in S1 (white arrowhead “a”) and spread rostrally (white arrowhead “b”) and ventrally (black arrowhead). (B) An example of excitatory propagation elicited by air puff stimulation of the nasal tip. Note that the first neural excitation was elicited in S1 (white arrowhead “c”) and spread rostrally (black arrowhead) and ventrally. (C) Temporal profiles of optical signals in the regions of interest (ROIs) indicated by black, red, and blue circles before, during and after nasal mucosa stimulation (gray bar) shown in (A). The green line shows the signal obtained from the ROI shown in nasal tip stimulation (B). (D) Lesions were made in the ROIs shown in (A) and (B). (E) Coronal Nissl sections showing the lesion of the arrowhead “a” (Ea), “b” (Eb), and “c” (Ec). Lower panels show the magnified images of the boxes in the upper panels. All data shown in Figure 1 were obtained from the same animal. IC, insular cortex; M, motor cortex; S1, primary somatosensory cortex; S2, secondary somatosensory cortex.

A population study for comparison of nasal mucosa-, nasal skin-, pharynx-, and tongue-responsive regions

To identify the precise region in response to the nasal mucosa within the S1 somatotopic map, pharynx- and tongue-responding regions were also examined, likewise their spatial arrangements in S1. I aligned each responding site on the cortical map standardized to the MCA and rhinal fissure (Fig. 2A) as previously reported (Kobayashi et al., 2010; Fujita et al., 2012, 2017).

Typical examples of excitatory areas are shown in Fig. 2A. Initial response to nasal tip stimulation was found caudal to responses of nasal mucosa stimulation (Fig. 2Aa and b). In contrast, initial response to pharynx stimulation occurred rostral to nasal mucosa-responding region (Fig. 2Ac). Moreover, tongue stimulation induced excitation more rostral to the pharynx-responding region (Fig. 2Ad).

To clarify this point, the initial responses to nasal mucosa ($n = 17$), nasal tip ($n = 17$), pharynx ($n = 6$), and tongue ($n = 6$) were superimposed using results that involved all data sets (Fig. 2B). Although the topographic organization of the initially activated area corresponding to each stimulus of peripheral region was not completely overlapped in reference to the rhinal fissure and MCA, all animals ($n = 17$) showed the characteristic topographical representation of the initial excitation responding to nasal mucosa and tip stimulation (i.e. the nasal mucosa-responding region was located rostral to the nasal tip-responding region; Fig. 2B; $p < 0.001$, binomial test). This would imply that there is a tendency for the tongue-, pharynx-, nasal mucosa-, and nasal tip-responding regions to be rostrocaudally arranged in S1. By aligning the nasal mucosa-responding regions, this topographic organization became clear as shown in Fig. 2C.

Frames obtained at 95% of the peak amplitude were superimposed in Fig. 2D which would suggest that the later responses were partially overlapped and that the nasal tip-, nasal mucosa-, and upper pharynx-responding regions look to be continuously located in S1. Tongue-responding region was less overlapped to that of the other regions which may reflect the spatial gap between the tongue and the upper pharynx. The temporal kinetics of excitation were compared among the responses to nasal mucosa, nasal tip, pharynx, and tongue stimulation in each initial responding site. The peak amplitude, time to peak, latency, rise time, decay time, and half duration were almost comparable among them except for the longer peak and rise time of tongue stimulation (Fig. 2E).

Stimulation intensity-dependent responses in S1 and S2

Peak amplitude and activated area increased in a stimulation intensity-dependent manner and plateaued at 20 psi in both S1 and S2 (Fig. 3A, B). The time to peak was shorter, in accordance with a larger intensity of the stimulus (Fig. 3B).

In the case of the air puff application at 25 psi, a rebound response occurred, whereby, the signal was increased at the termination of the stimulus (Fig. 3B, arrowhead). The rebound responses were less prominent, which was in accordance with the smaller intensity of the

stimuli. It should also be noted that the strong stimulus induced oscillation-like activities in the initial response region (Fig. 3B).

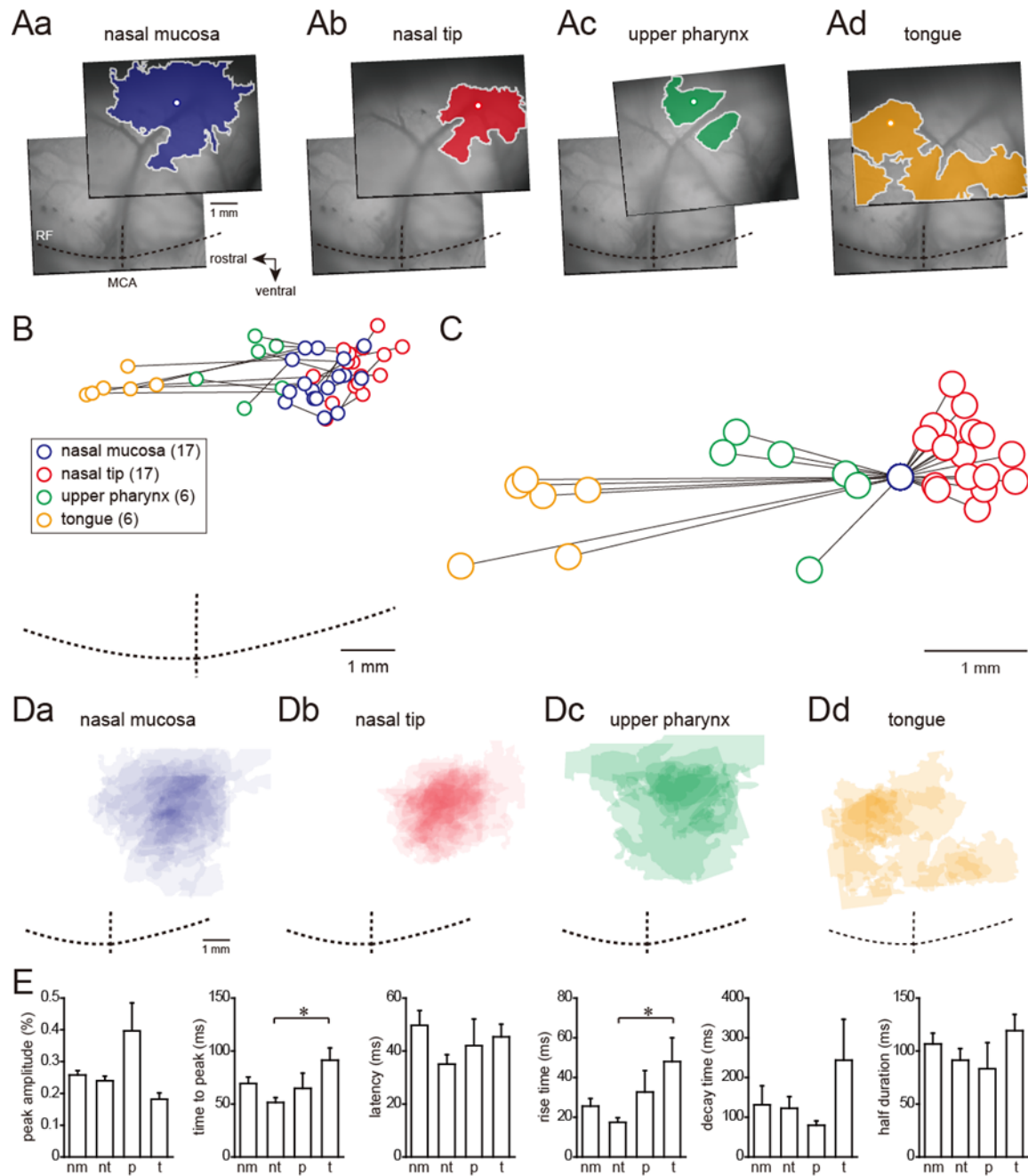


Figure 2. Comparison of spatiotemporal profiles of responses to nasal mucosa, nasal tip, upper pharynx, and tongue stimulation. (A) Examples of excitation obtained from the frame showing 95% peak amplitude evoked by air puff stimulation (20 psi) to the nasal mucosa (Aa), nasal tip (Ab), upper pharynx (Ac), and tongue (Ad). Locations of initial responses are depicted by circles. (B) Locations of the initial excitation are superimposed in reference to the MCA and rhinal fissure (RF). Blue, red, green, and orange circles with lines indicate the location of the initial responses to nasal mucosa, nasal tip, upper pharynx, and tongue stimulation in each animal. (C) Initially excited regions to the nasal mucosa (blue circles shown in B) are aligned to clarify the comparative topographic feature of the initially activated regions in response to nasal tip, upper pharynx, and tongue stimulation. Note that all initial responses to nasal tip and pharynx stimulation are located caudal and rostral to those to nasal mucosa stimulation, respectively. (D) Superimposed images of the responses at 95% of peak amplitude. Number of overlapping responses is represented by the density of color. (E) Comparison of the peak amplitude, time to peak, latency, rise time, decay time, and half duration of excitation obtained in the location of the initial response among nasal

mucosa (nm), nasal tip (nt), upper pharynx (p), and tongue (t) stimulation. * $p < 0.05$, ANOVA on ranks with Dunn's method.

Summary of peak amplitudes and activated areas is shown in Fig. 3C ($n = 8$). The peak amplitude in the initial and secondary responding regions increased in a stimulation intensity-dependent manner up to 20 psi ($p < 0.01$, ANOVA or ANOVA on ranks) and the area of the cortical response reached plateau at 20 psi.

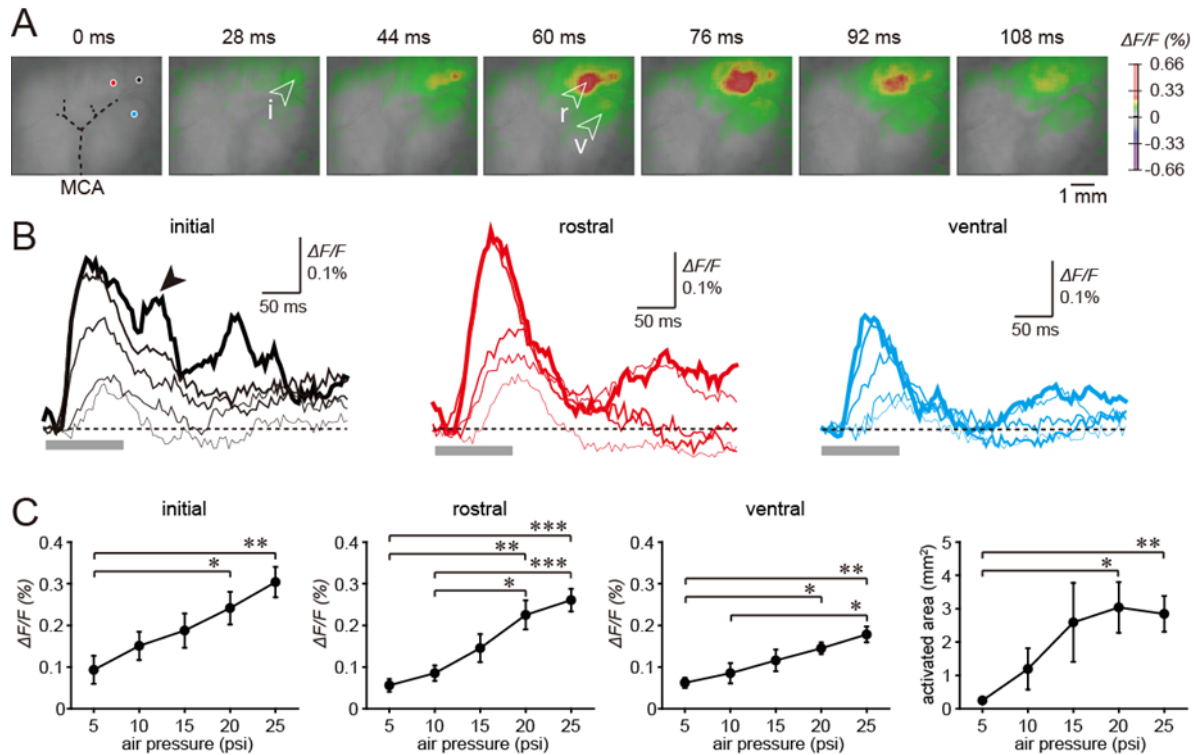


Figure 3. Air pressure intensity-dependent responses to nasal mucosa stimulation. (A) An example of excitatory propagation elicited by air puff stimulation (20 psi) of the nasal mucosa. Note that the initial response was elicited in S1 (arrowhead “i”) and spread rostrally (arrowhead “r”) and ventrally (arrowhead “v”). (B) Temporal profiles of optical signals in the ROIs indicated by black, red, and blue circles in (A). Thickness of lines indicate intensity of air pressure; five lines from thin to thick indicate 5, 10, 15, 20, and 25 psi. Gray bars indicate the period of air puff application. Note the air pressure intensity-dependent increase in the amplitude of signals and the hump at the termination of air puff application at 25 psi (arrowhead). (C) Optical signals in response to nasal mucosa stimulation and activated areas are significantly increased dependent on the air pressure (** $p < 0.001$, ** $p < 0.01$, * $p < 0.05$, ANOVA or ANOVA on ranks with Tukey test).

Odor stimulation

Most odorants induce simultaneous activation of the olfactory and trigeminal systems, and recent studies have reported an interaction between the two (Sant'Ambrogio et al., 1995; Brand, 2006; Croy et al., 2014). To examine the effect of odor on S1 excitation induced by the contralateral air puff application, I compared the peak amplitude of S1 excitation between the puff application of the deodorized air and amyl acetate (Fig. 4). Pressure of the puff application was set at 10-15 psi, which induced the mild increase in the excitation amplitude, to detect both an increase and a decrease in the amplitude.

Both the puff application of the air without (Fig. 4Aa) and with amyl acetate (Fig. 4Ab) to the contralateral nasal mucosa induced the excitation in the similar S1 region, and the

amplitude of the excitation was comparable (Fig. 4B). Fig. 4C shows a summary result of the amplitude of excitation in S1 without and with amyl acetate which indicates no significant difference between them ($n = 8$; $p = 0.742$, Wilcoxon signed-rank test). This result suggests the negligible convergence of somatosensory and olfactory sensation in the contralateral S1.

Response in the piriform cortex

To examine the effect of the air puff stimulation with and without amyl acetate on the olfactory system in the present experimental condition, I performed optical imaging focusing on the piriform cortex located around the MCA. It should be noted that the trigeminal system is principally mediated by the contralateral S1, whereas, the olfactory system possesses an ipsilateral dominance. Thus, I examined the effects of air puff stimulation of the ipsilateral nasal mucosa.

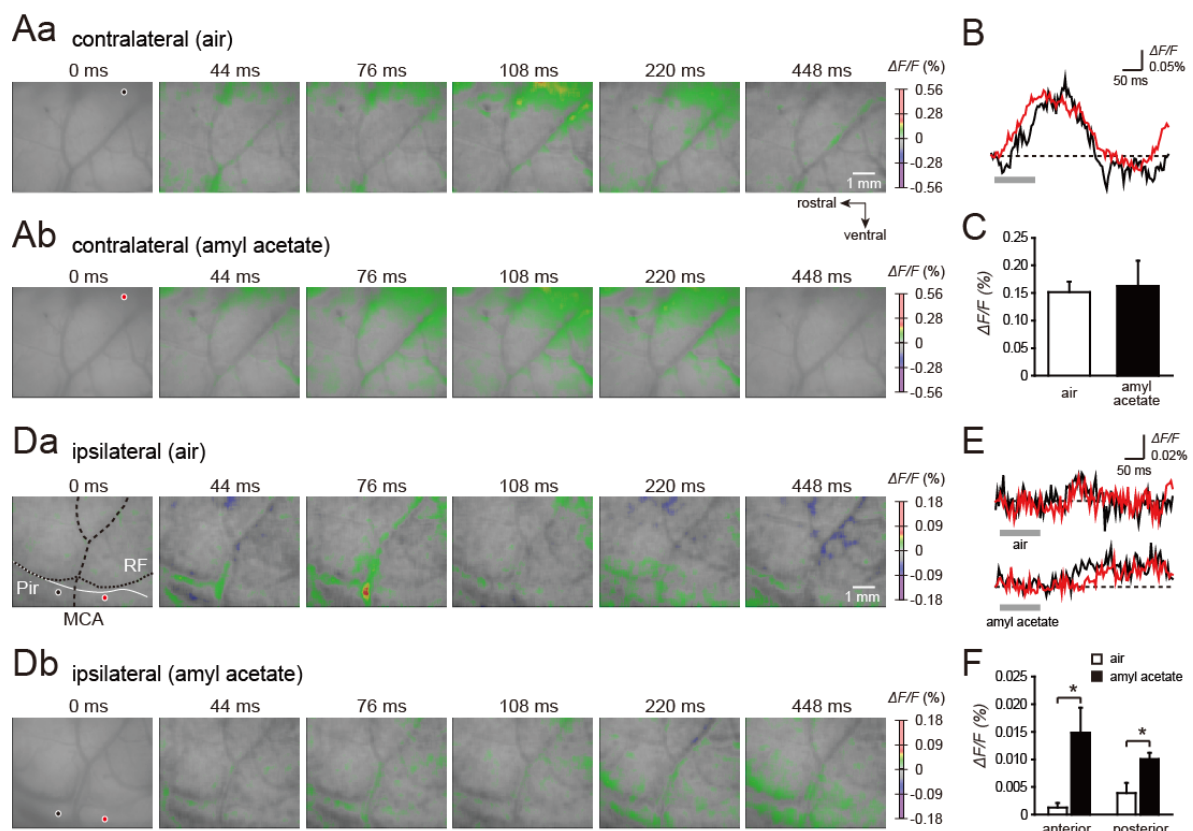


Figure 4. Responses to air puff stimulation (10-15 psi) of the nasal cavity with and without amyl acetate. (A) Examples of excitatory propagation in response to contralateral nasal mucosa stimulation without amyl acetate (Aa) and with amyl acetate (Ab) in S1. (B) Temporal profiles of optical signals in the ROIs indicated by black (air) and red circles (amyl acetate) in (A). (C) Peak amplitudes in S1 are comparable between air and amyl acetate. (D) Examples of excitation in the piriform cortex (Pir) responding to ipsilateral nasal mucosa stimulation without (Da) and with amyl acetate (Db). Note the higher gain than that of (A). (E) Temporal profiles of optical signals in the ROIs indicated by black (anterior) and red (posterior) circles in (D). Note that amyl acetate induced faint and persisting excitation in the piriform cortex. (F) Amplitude of increase in optical signal induced by amyl acetate is higher than that by the deodorized air. $*p < 0.05$, paired t -test.

Ipsilateral deodorized air puff stimulation evoked a negligible increase in the optical signal of the piriform cortex (Fig. 4D-F). After a puff application of amyl acetate, a faint

persisting increase in optical signal in the piriform cortex was observed (Fig. 4E). A significant increase in the optical signal of the piriform cortex evoked by puff applications of amyl acetate in comparison to that by the deodorized air application ($n = 7$; anterior, $p < 0.05$; posterior, $p < 0.05$, paired t -test; Fig. 4F) insinuates that the odor stimulation in this study certainly activates the olfactory system.

Discussion

The present study demonstrated the spatiotemporal profiles of neural excitation induced by nasal mucosa, nasal tip, pharynx, and tongue stimulation. Response to nasal mucosa stimulation by application of an air puff initially elicited activation in part of S1 rostral to that of nasal tip stimulation. In the later responses, the nasal mucosa stimulation-induced excitation spread to ventrally and rostrally adjacent regions which corresponded to S2 and the upper pharynx-responding region in S1, respectively. Optical signal in the piriform cortex was slightly increased by ipsilateral puff stimulation with amyl acetate. On the other hand, stimulation with amyl acetate induced a comparable excitation in S1 compared to air puff stimulation which suggests that optical signals in S1 primarily represents the information processing from trigeminal but not olfactory system. Meanwhile, the kinetics of the optical signal, including the amplitude, time to peak, latency, rise time, decay time, and half duration in the center of the initial response were almost comparable among nasal mucosa, nasal tip, pharynx, and tongue stimulation. The spatial localization of the S1 regions corresponding to the nasal mucosa, nasal tip, pharynx, and tongue indicates the somatotopic organization of not only the outer (skin) but also the inner (mucosa) surface of the face which in-turn suggests a functional organization of the somatosensory information processed in S1.

Peripheral nervous system conducts somatosensory information from the nasal cavity

The nasal cavity is innervated by the ophthalmic and maxillary nerves, which are branches of the trigeminal nerve (Tsubone, 1989; Sant'Ambrogio et al., 1995; Brand, 2006). The internal nasal branch of the anterior ethmoidal nerve, which is a branch of the ophthalmic nerve, provides sensory branches to the anterior part of the inner nose (i.e., the nasal vestibule and mucosa of septum), whereas the alae nasi is innervated by the external nasal branch (Bojsen-Møller, 1975; Tsubone 1989; Sant'Ambrogio et al., 1995). Thus, the sensory information conveyed to the nasal cavity due to an air puff stimulus is likely conducted by the internal branch of the anterior ethmoidal nerve. Tsubone (1989) demonstrated that the ethmoidal nerve is activated during airflow and tactile stimulation in rats. Furthermore, the vast majority (86%) of pressure-responsive fibers are activated exclusively by negative pressure while the rest is also stimulated by positive pressure, although negative pressure has a greater effect (Tsubone, 1990; Sant'Ambrogio et al., 1995). My finding of a rebound response induced at the termination of the air puff stimulus (Fig. 3B) supports this notion, as the rebound response is likely to elicit negative pressure in the nasal cavity.

S1 and S2 responses to air puff stimulation of the nasal cavity

A previous human fMRI study indicates that the tactile information from the nasal mucosa is processed in S1 close to regions that process information from the alar wing of the nose (Gastl et al., 2014). In the present study, I demonstrated that localizations of the inner nose, nasal mucosa, and outer nose, nasal tip, were similarly adjacent in rats. The S1 region of the nasal tip in this study appears to correspond to the results of previous studies (Waite and Taylor, 1978; Rempel et al., 2003; Yu et al., 2010). In all cases, the initial responses to nasal mucosa stimulation began consistently in regions rostral to the initial responses to nasal tip stimulation and responses are likely to be located without spatial separation (Fig. 2A-D).

Application of an air puff to the nasal cavity evoked neural excitation in the ventral part of S1 and spread in a rostral and ventral direction. The upper pharynx is continuous with and located caudal to the nasal cavity. Thus, the air puff may stimulate not only the nasal mucosa but also the upper pharynx. This hypothesis was supported by the finding that the air puff stimulation of upper pharynx induced excitation in the rostral region adjacent to the initially activated region responding to the nasal mucosa stimulation (Fig. 2B,C). Such continuous topographic organization of the inner nose and pharynx in S1 have been reported by fMRI and PET studies in human which demonstrates the close localization of the nasal mucosa to the pharynx (Albrecht et al., 2010; Gastl et al., 2014).

S2 is located ventral to S1, like a mirror image with an axis of symmetry that is the border of the facial areas of S1 and S2 (Rempel et al., 2003; Benison et al., 2007). Thus, the spread of excitation in a ventral direction from the initially activated region in S1 likely represents the transmission of information from S1 to S2. Subsequent activation of S2 suggests that somatosensory inputs to the nasal mucosa are processed initially in S1, followed by the flow of information from S1 to S2.

In addition to the localization of the outer and inner nose, I examined the kinetics of responses to nasal mucosa, nasal tip, pharynx, and tongue stimulation. Kinetics of the optical signal, including the peak amplitude, time to peak, latency, rise time, decay time, and half duration in the region of the initial response were almost comparable among them (Fig. 2E). This result implies that information from these areas is processed in temporally similar fashion in S1.

Odor effect on cortical activities

Olfactory and trigeminal nervous systems interact in nasal chemoreception (Sant'Ambrogio et al., 1995; Brand, 2006; Croy et al., 2014) and a human fMRI study demonstrated a critical role of the trigeminal system in the identification of odor localization (Croy et al., 2014). Although the application of air with amyl acetate slightly activated the ipsilateral piriform cortex, the excitation of the contralateral S1 induced by the air puff was less influenced by adding amyl acetate. These findings suggest that the interaction between

the somatosensory and olfactory systems is relatively small in the contralateral S1, at least in the event that the duration of somatosensory and olfactory stimuli is relatively shorter (in ms order) than that of respiration (in s order). In other words, the S1 map in this study can be considered as representation of information processing in the trigeminal nervous system. My results do not exclude the possibility that the information from the olfactory and trigeminal nervous systems converge in ipsilateral S1, S2, and other regions which should be addressed in future studies.

Technical limitations of the experiments

In spite of the consistency of the rostrocaudal spatial distribution of the nasal mucosa- and tip-responding regions, there was a variation in the activated region as shown in Fig. 2B. Several possibilities for this result exist.

The first possibility is the variation of the stimulated regions. Air puff stimulation enables repeated stimulation of targeted areas with high temporal activation and has the advantage of being non-invasive. For example, bleeding may occur due to the insertion of a stimulation electrode in the nasal cavity. However, the air puff stimulus might stimulate a broader area compared to electrical stimulation. Second, the effects of thick vessels are still not negligible in *in vivo* optical imaging even though RH-1691 is a voltage-sensitive dye that was developed to reduce the artifact caused by hemoglobin absorbance (Civillico and Contreras, 2005; Lippert et al., 2007). Indeed, my data showed that the signals on thick vessels, including the MCA, did not exceed the threshold level due to artifact. Thus, the thick vessels might have made a slight shift to the center of the detected activation region.

Functional implications

The regions that responded to stimulation of the inner and outer nose in rats were located in adjacent cortical regions, as I hypothesized. Localization of the responding region to the nasal mucosa was consistently rostral and caudal to the nasal tip-responding and pharynx-responsive regions, respectively. Taking into account the overlap of the maximum responses of the nasal mucosa and these regions, these cortical regions appear to be connected and each affect the activity of the other. S1 serial activation from the nasal tip to the upper pharynx may be important in the identification of the direction and pressure of air flow, as well as, the temperature and humidity of the air during respiration.

Somatosensory information from the nasal cavity is involved in various respiratory reflexes (Tsubone, 1989). For example, probing the nasal cavity as well as electrical stimulation of the ethmoidal nerve induces sneezing in anesthetized guinea pigs (Sekizawa et al., 1998). Additionally, air-jet stimulation of the nasal cavity decreases the activity of the major inspiratory muscles in decerebrate cats (Enomoto et al., 1998). This reflex might also contribute to avoiding the inspiration of dust. In this context, the serial activation of the S1 region is likely to play a role in biophylaxis.

Chapter 2

Preceding administration of minocycline suppresses neuroplastic changes in cortical excitatory propagation in the model rat with partial infraorbital nerve ligation

Introduction

The trigeminal nerve has three major branches, the ophthalmic, maxillary, and mandibular nerves. The infraorbital nerve (ION) is a branch of the maxillary nerve, which innervates to the middle part of the maxillofacial region including the whisker pad. Partial ligation of ION (pl-ION) induces changes in spontaneous behaviors and responses to mechanical stimulation (Vos et al., 1994; Xu et al., 2008). The animal with pl-ION shows lower threshold for a brisk withdrawal of the head responding to mechanical stimulation of the ipsilateral whisker pad, and allodynia starts from one day (1 d) after pl-ION and sustains more than 3 weeks (Xu et al., 2008). Interestingly, allodynia also occurs in the surrounding region of the pl-ION and in the contralateral whisker pad (Xu et al., 2008), indicating that ectopic pain occurs in the pl-ION model.

The dorsal part of the insular cortex (IC) around the middle cerebral artery (MCA) and the adjacent secondary somatosensory cortex (S2) receive sensory information from the oral structures including the dental pulp (Nakamura et al., 2015, 2016) and the periodontal ligament (Horinuki et al., 2015, 2016). The S2 and IC related to the sensation in the oral structure (S2/IO) project to the limbic structures such as amygdala (Allen et al., 1991; Shi and Cassell, 1998) and lateral hypothalamic area (Allen et al., 1991). In addition, the recent anatomical studies have demonstrated the descending projections to the trigeminal spinal subnucleus caudalis (Vc), which receives nociceptive inputs from the orofacial structures (Takemura et al., 2006) and transmits these information to the higher brain regions including the parabrachial nucleus and thalamus (Mitchell et al., 2004). Therefore, S2/IO is considered to play a key role in nociceptive information processing of the oral structures (Kobayashi and Horinuki, 2017).

Recent studies have demonstrated that disturbance of nociceptive inputs induces neuroplastic changes not only in the peripheral but also in the central nervous system including the cerebral cortex, and such neuroplastic changes in the cortex may be a part of mechanisms underlying the refractory pain (Qiu et al., 2013). Indeed, trigeminal nerve injury causes neuroplastic changes in neural responses of S2/IO. I have demonstrated that 1-2

weeks after transection of the inferior alveolar nerve, a branch of the mandibular nerve, S2/IOR shows hyperexcitability responding to electrical stimulation of the upper molar pulp, which is innervated by the maxillary nerve (Fujita et al., 2019). A part of the mechanisms for this neuroplastic change occur in the local circuits of S2/IOR. This finding suggests a possibility that hyperexcitability of S2/IOR may trigger chronic pain even after recovery of the peripheral nervous system that is directly damaged.

Not a few studies in terms of the injury models of the trigeminal nerve have reported the substances that suppress pain-related behaviors. Activation of microglial cells is considered to be a key process that induces neuropathic pain. A variety of cytokines and neurotrophic factors have been reported to induce neuroplastic changes and central sensitization noted above (Latremoliere et al., 2008; Taylor and Ribeiro-da-Silva, 2011). However, little information is available how these molecules affect on neural activities in the cerebral cortex. Taking that the cortical responses reflect integrated information from the peripheral nerve to the cerebral cortex, clarification of molecules effects on cortical responses provides critical information of the mechanisms for suppression of nociception.

Minocycline is one of the microglial inhibitors, and the present study aimed to elucidate the effect of minocycline application to the pl-ION model on hyperexcited cortical activities in S1/2 and IC. I performed an in vivo optical imaging with RH1691, a voltage-sensitive dye, under urethane anesthesia. The amplitude of optical signals mediated by the voltage-sensitive dye correlates to the membrane potential and reflects excitatory and inhibitory postsynaptic potentials in real time (Berger et al., 2007), and thus, I can quantify the spatiotemporal patterns of neural excitation with a high resolution. The findings obtained from this study shed light on a new approach to prevent chronic pain induced by peripheral nerve injury.

Materials and Methods

The Animal Experimentation Committee of Nihon University approved the present experiments, which were performed according to the institutional guidelines for the care and use of experimental animals described in the National Institute of Health Guide for the Care and Use of Laboratory Animals. All efforts were made to minimize animal suffering and to reduce the number of animals used.

Animals

Four to five-week-old male Wistar rats (Sankyo Labo, Tokyo, Japan) were anesthetized with intraperitoneal (i.p.) administration of butorphanol (2.5 mg/kg, Meiji Seika Pharma, Tokyo, Japan), medetomidine (0.375 mg/kg, Zenocq, Fukushima, Japan), and midazolam (2.0 mg/kg, Sandoz, Tokyo, Japan) dissolved in saline. A pl-ION was performed via the oral cavity (Shinoda et al., 2007). Briefly, gingivobuccal fold was incised to expose the ION (Fig. 1A). An one-half to one-third thickness of the ION was trapped and ligated tightly by 5-0 silk. The incision was sutured with 5-0 silk. The sham operation was identical except for nerve

ligation.

In the model of minocycline treatment, minocycline hydrochloride (30 mg/kg/d, i.p.; Sigma-Aldrich, St Louis, USA) was daily administered from 1 d before pl-ION to 2 d after pl-ION. The 3d-pl-ION received saline injection instead of minocycline.

Behavioral test

The head-withdrawal threshold (HWT) to mechanical stimulation of the ipsilateral whisker pad skin was measured using von Frey filaments (4, 8, 15, 26, 30, 40, 50, 60, and 100g of force; North Coast Medical, Morgan Hill, USA) before and 1, 3, 7, and 14 d after pl-ION (Fig. 1B). The animals were restrained around the trunk with a cloth to calm them and were treated gently during the experiments. Training sessions were performed for at least 7 consecutive days. Each stimulus was applied 5 times in each series of trials. HWT for mechanical stimulation was determined as the minimum pressure intensity that evoked head-withdrawal behavior in response to more than 3 of 5 stimuli. All behavioral tests were performed under blinded conditions.

In vivo cerebrocortical imaging

Optical imaging was performed as previously described (Horinuki et al., 2015, 2016; Nakamura et al., 2015, 2016; Kaneko et al., 2017, 2018; Zama et al., 2018; Fujita et al., 2019). Briefly the sham and pl-ION model rats were anesthetized with urethane (1.5 g/kg, i.p.), and then, atropine methyl bromide was administered (0.5 mg/kg, i.p.). The toe pinch reflex was monitored to check the depth of anesthesia, and additional urethane was administered as needed. Body temperature was kept at 37°C using a rectal probe and heating pad (BWT-100, Bio Research Center, Osaka, Japan). The local anesthetic, lidocaine (2% gel, AstraZeneca, Tokyo, Japan), was administered to the skin before incision. The anesthetized rats were fixed to a custom-made stereotaxic snout frame (Narishige, Tokyo, Japan), which was tilted 60° laterally, and a craniotomy was performed (Fig. 1C).

RH1691 (1 mg/ml; Optical Imaging, New York) in saline was applied to the cortical surface for 1 hour. This application method of RH 1691 stains cells between the cortical surface and the deeper layer III. Thus, the optical signals reflect changes in the membrane potential of neurons in layers I–III (Nakamura et al., 2015). Changes in RH1691 fluorescence were measured using the CCD camera (MiCAM02, Brainvision, Tokyo, Japan), which was mounted on a stereomicroscope (Leica Microsystems, Wetzlar, Germany). The cortical surface was illuminated through a 632-nm excitation filter and a dichroic mirror using a tungsten-halogen lamp (CLS150XD, Leica Microsystems). The fluorescent emission was captured through an absorption filter ($\lambda > 650$ -nm longpass, Andover, Salem, MA). The size and resolution of the image captured with the CCD camera was 6.4×4.8 mm² and 184×124 pixels, respectively.

To remove signals due to acute bleaching of the dye, values without stimuli were subtracted from each recording with stimulation. The sampling interval was 4 ms (250 Hz),

and the acquisition time was 500 ms, which was mostly longer than 90-10% decay time of optical signals responding to the stimulation. Forty consecutive images were averaged to improve signal to noise ratio.

Stimulation of the skin and dental pulps

To quantify the cortical excitation responding to electrical stimulation of the regions innervated by the maxillary and mandibular nerves, I inserted bipolar electrodes, which were made from enamel-coated copper wire (diameter = 80 μm), into the whisker pad skin, mandibular first molar pulp (Fig. 1C), and mentum skin (Nakamura et al., 2015). Five rectangular voltage pulses (5 V, 100- μs duration, 20 ms interstimulus interval) were applied by a stimulator (STG2008, Multi-Channel Systems, Reutlingen, Germany) at 0.05 Hz to obtain stable cortical responses.

Data analysis

The optical imaging data were processed and analyzed using Brain Vision Analyzer software (Brainvision, Tokyo, Japan). Changes in the intensity of fluorescence (ΔF) of each pixel relative to the initial intensity of fluorescence (F) were calculated ($\Delta F/F$), and the ratio was processed with a spatial filter (9×9 pixels). A significant response was defined as a signal exceeding 7 times the SD of the baseline noise, as previously described (Nakamura et al., 2015). Images were aligned across multiple rats using the rhinal fissure and MCA as landmarks. In a part of animals, the rhinal fissure and the MCA could not be aligned with the other animals due to angioplany; therefore, I excluded the results obtained from these animals. I estimated the spatial profiles of excitation using the initial and maximum responses. The initial response was obtained by outlining the excitation evoked in the first frame that exhibited a significant increase in the optical signal. The maximum response was defined as the outline of the excitatory response in the frame with the maximum amplitude of the optical signal in the center of the initial response. I defined the peak amplitude at the maximum amplitude of an optical response at the point of the initial response.

Statistics

The data are expressed as the mean \pm SEM. Student's t-test was used in the analyses. In multiple comparisons, I applied the Bonferroni correction with a Bonferroni-corrected probability value of $p < 0.016$ considered statistically significant.

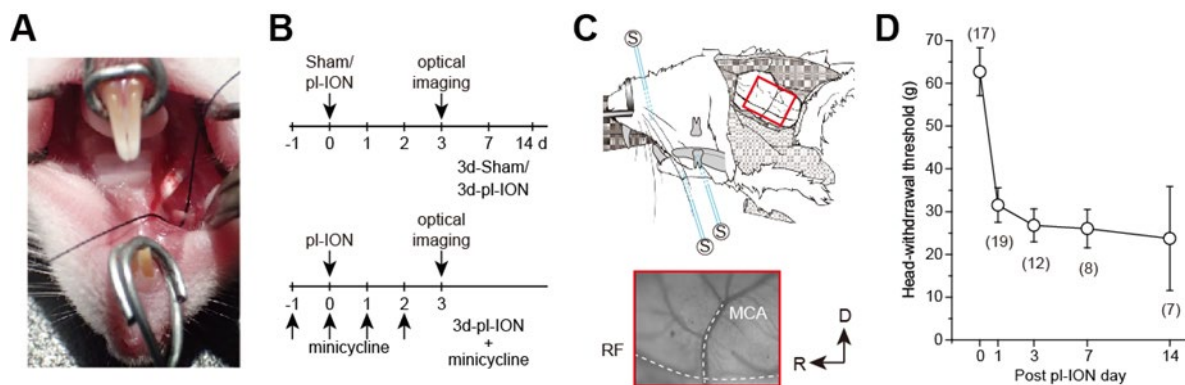


Figure 1. Experimental protocols for partial ligation of the infraorbital nerve (pl-ION) and optical imaging. (A) An intraoral approach to expose ION. A black silk thread was placed under ION to show ION clearly. (B) Experimental schedules. On 0 d, pl-ION was performed, and a behavioral test was performed 1, 3, 7, and 14 d after pl-ION. Optical imaging was performed 3d after pl-ION. In the group administrated with minocycline, minocycline (30 mg/kg/d) was intraperitoneally injected from 1 d before and 2 d after pl-ION. (C) Schematic drawing of the in vivo preparation for the optical imaging and position of the stimulation electrodes (modified from Fujita et al. 2010 with permission). The lower panel indicate an example of the image of the cortical surface including S1 and S2/IO. MCA, middle cerebral artery; RF, rhinal fissure. R, rostral; D, dorsal. (D) The temporal profile of head-withdrawal threshold (HWT) before and after pl-ION. The number in the parenthesis indicates the number of animals.

Results

Temporal changes in HWT of pl-ION models

Head-withdrawal reflex elicited by mechanical stimulation using von Frey filaments was examined to evaluate nociceptive threshold in pl-ION models. HWT of nociceptive responses to the application of von Frey filaments showed a significant decrease 1-14 d after pl-ION in comparison to that before pl-ION, indicating the development of mechanical hyperalgesia (Fig. 1D). Clinically, it is considered that treatments of neuropathic pain are more effective in the earlier period, and thus, I focused on the profile 3 d after pl-ION in the following analyses.

Cortical responses to electrical stimulation of the whisker pad skin

ION innervates to the whisker pad skin, and pl-ION injured a part of ION. To examine the effect of pl-ION on the cortical activities, I first stimulated the whisker pad skin using a bipolar electrode.

The responses were consistently observed in the barrel field that involves both S1 and S2 responding to electrical stimuli at 5 V (Fig. 2A and B) as previously reported (Remple et al., 2003; Nakamura et al., 2015). The excitation in S1 and S2 frequently expanded beyond the field of view, and thus I quantified only the amplitude of excitation in the initially evoked response region. Because of the difficulty in identifying the border between S1 and S2, I quantified the amplitude in the initial region of excitation as the representative amplitude in S1/S2. For the comparison to the excited regions responding to whisker pad skin stimulation, I first imaged IC around MCA, which corresponds to IO, and then moved the field of view dorsally to image the barrel cortex.

The peak amplitudes of cortical excitation in S1/S2 of 3d-Sham were $0.89 \pm 0.08\%$ (N =

18). Cortical excitation 3 d after pl-ION was significantly reduced to $0.60 \pm 0.07\%$ ($N = 13$; $p < 0.016$, Student's t-test with Bonferroni correction; Fig. 2C). There was little difference in the evoked S1/S2 regions between 3d-Sham and 3d-pl-ION as shown in Fig. 2D. These results suggest that pl-ION decreases somatosensory sensation 3 d after the treatment.

Cortical responses to electrical stimulation of the mandibular molar pulp

The mandibular first molar pulp is innervated by the inferior alveolar nerve, a branch of the mandibular nerve, which is adjacent to the maxillary nerve but is not injured in the present experimental condition. To test whether pl-ION induces ectopic pain as previously reported in similar nerve injury models (Shibuta et al., 2012; Fujita et al., 2019), I examined the profiles of cortical responses to the mandibular molar pulp stimulation.

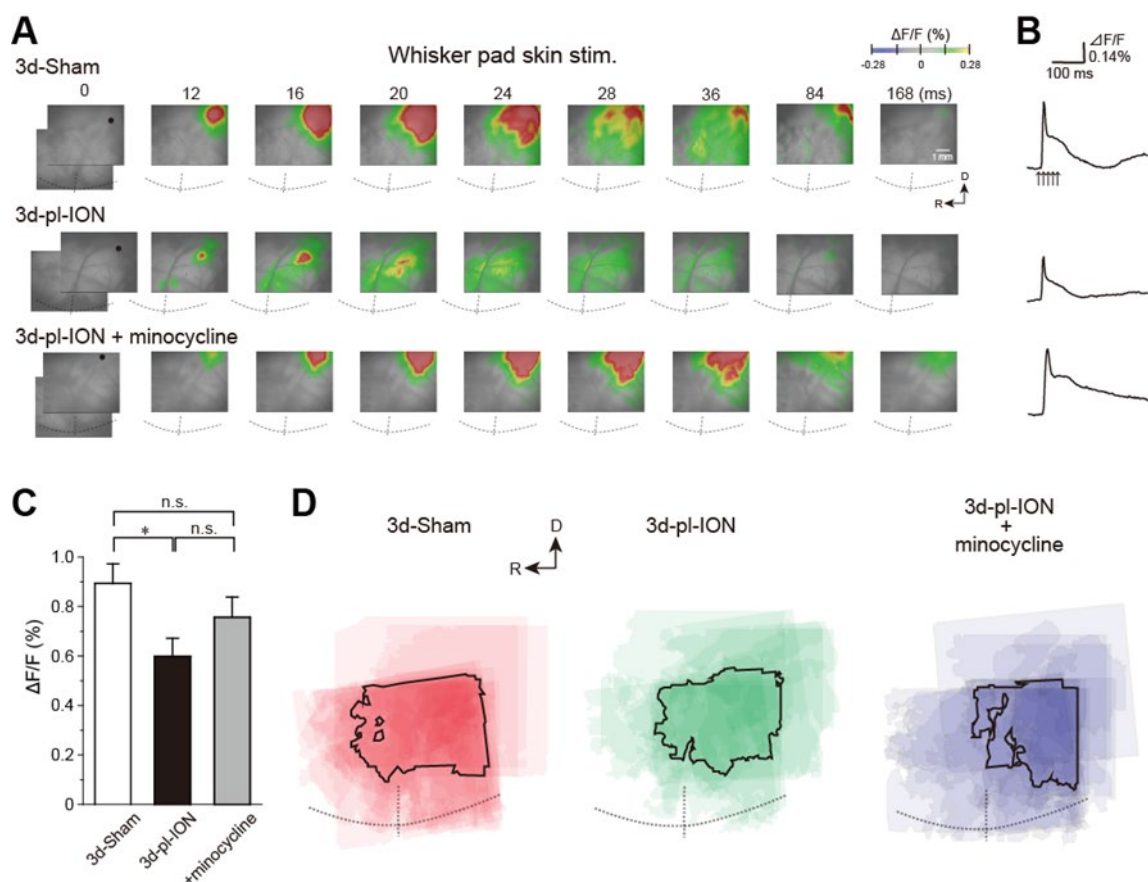


Figure 2. Cortical responses to electrical stimulation of the whisker pad skin. (A) Representative examples of cortical responses in 3 d after sham operation (3d-Sham), 3 d after pl-ION (3d-pl-ION), and 3d-pl-ION that received minocycline administration (3d-pl-ION+minocycline). The time from the onset of the electrical stimulation of the whisker pad skin is shown on the top of each panel. R, rostral; D, dorsal. (B) Temporal profiles of optical signals in the regions of interest (ROIs; black circles) in S1/S2 shown in (A). (C) The amplitude of S1/S2 excitation in 3d-Sham ($N = 18$), 3d-pl-ION ($N = 13$), and 3d-pl-ION with minocycline ($N = 15$). (D) Superimposed images of the maximum responses evoked by the whisker pad skin stimulation. The number of overlapping responses is represented by gradation of the color density. The line outlines the area responding to stimulation in 50% of animals. $*p < 0.016$, Student's t-test with Bonferroni correction.

The initial responses to electrical stimulation of the mandibular molar pulp were detected in two cortical regions: the rostroventral part of S1 and dorsocaudal part in reference to the

cross point of the rhinal fissure and MCA (Fig. 3A and B). The latter corresponds to S2/ IOR as previously reported (Nakamura et al., 2015, 2016). Excitation spread to the surrounding cortical regions in a concentric manner. Similar to the case of the whisker pad skin stimulation, I stimulated the molar pulps at 5 V because the responses in S1 and S2/IOR was consistently observed at 5 V (Nakamura et al., 2015).

In 3d-Sham, the peak amplitudes of cortical excitation in S1 and S2/IOR were $0.27 \pm 0.05\%$ (N = 13) and $0.21 \pm 0.04\%$ (N = 13), respectively. Cortical excitation 3 d after pl-ION was facilitated in both S1 and S2/IOR (Fig. 3E). In 3d-pl-ION, the peak amplitude of cortical excitation in S1 was significantly larger than that in 3d-Sham ($0.54 \pm 0.08\%$, N = 13; $p < 0.016$, Student's t-test with Bonferroni correction). Similarly, S2/IOR showed larger cortical excitation in 3d-pl-ION than that of the Sham ($0.55 \pm 0.06\%$, N = 13; $p < 0.001$, Student's t-test with Bonferroni correction). These results suggest that ectopic pain occurs in 3d-pl-ION.

Cortical responses to electrical stimulation of the mentum skin

The skin is consistently stimulated, whereas the dental pulps are protected from mechanical stimulation by the dentin and enamel. These differences might cause a distinct effect of pl-ION on evoked cortical responses between the skin and dental pulps, although stimulation of the dental pulps by the bipolar electrodes has an advantage to restrict the stimulated region. I, therefore, examined the cortical responses to stimulating the mentum skin, which is innervated by the mental nerve, a branch of the mandibular nerve.

In 3d-Sham, the peak amplitudes of cortical excitation in S1 and S2 were $0.36 \pm 0.05\%$ (N = 7) and $0.17 \pm 0.07\%$ (N = 7), respectively. Cortical excitation 3 d after pl-ION was facilitated in both S1 and S2/IOR (Fig. 3C, D, and F). In 3d-pl-ION, the peak amplitude of cortical excitation in S1 was significantly larger than that in 3d-Sham ($0.59 \pm 0.04\%$, N = 15; $p < 0.016$, Student's t-test with Bonferroni correction). Similarly, S2/IOR in 3d-pl-ION showed larger cortical responses to the mentum skin stimulation than that in 3d-Sham ($0.46 \pm 0.05\%$, N = 15; $p < 0.001$, Student's t-test with Bonferroni correction). These results suggest ectopic pain occurs 3d-pl-ION that not only in the dental pulp but also in the skin.

Minocycline partially recovers abnormal cortical responses to electrical stimulation of the orofacial regions

In the experiment of whisker pad stimulation, administration of minocycline (30 mg/kg; i.p.) once a day from a day before and 0, 1, and 2 d after pl-ION (Fig. 1B) tended to recover pl-ION-induced change in the amplitude of the cortical excitation in S1/S2 to 3d-Sham though the difference was not significant ($0.76 \pm 0.08\%$, N = 15; $p = 0.17$, Student's t-test with Bonferroni correction; Fig. 2). Indeed, no significant difference was detected in the comparison to 3d-Sham and to 3d-pl-ION with minocycline ($p = 0.24$, Student's t-test with Bonferroni correction).

On the other hand, minocycline decreased pl-ION-induced hyperexcitation of cortical responses to mandibular molar pulp and mentum skin stimulation (Fig. 3). In

minocycline-administered animals, mandibular molar pulp stimulation induced comparable cortical excitation in S1 compared to that of 3d-Sham ($0.38 \pm 0.05\%$, $N = 14$; $p = 0.15$, Student's t-test with Bonferroni correction), though this amplitude was not different from that in 3d-pl-ION ($p = 0.09$, Student's t-test with Bonferroni correction). In S2/IO, the group of 3d-pl-ION with minocycline showed a tendency of slightly higher amplitude of cortical excitation ($0.36 \pm 0.05\%$, $N = 14$) to that in 3d-Sham ($p = 0.03$, Student's t-test with Bonferroni correction), and this amplitude was significantly smaller than that in 3d-pl-ION ($p < 0.016$, Student's t-test with Bonferroni correction).

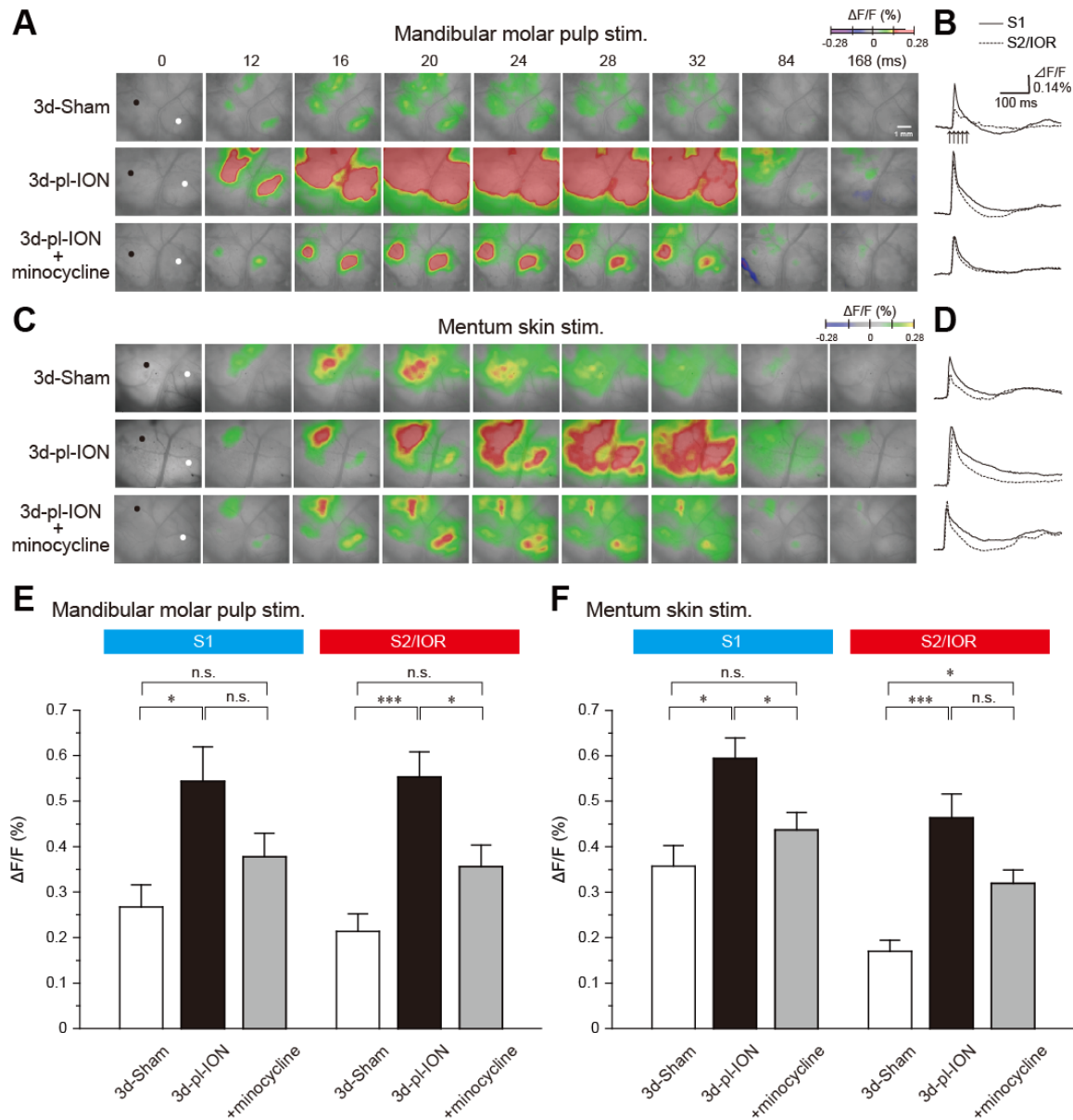


Figure 3. Cortical responses to electrical stimulation of the mandibular molar pulp and mentum skin. (A) Representative examples of cortical responses in 3d-Sham, 3d-pl-ION, and 3d-pl-ION+minocycline to mandibular molar pulp stimulation. The time from the onset of the electrical stimulation of the whisker pad skin is shown on the top of each panel. (B) Temporal profiles of optical signals in the ROIs: black circles in S1 (thick lines) and white circles in S2/IO (dotted lines) shown in (A). (C) Representative examples of cortical responses in 3d-Sham, 3d-pl-ION, and 3d-pl-ION+minocycline to mentum skin stimulation. (D) Temporal profiles of optical signals in the ROIs: black circles in S1 (thick lines) and white circles in S2/IO (dotted lines) shown in (C). (E) The amplitude of S1 (blue) and S2/IO (red) excitation in 3d-Sham ($N = 13$), 3d-pl-ION ($N = 13$), and 3d-pl-ION with minocycline ($N = 14$) in response to stimulation of the mandibular molar pulp. (F) The amplitude of S1 (blue) and S2/IO (red) excitation in

3d-Sham (N = 7), 3d-pl-ION (N = 15), and 3d-pl-ION with minocycline (N = 15) in response to stimulation of the mentum skin. * $p < 0.016$, *** $p < 0.001$, n.s. not significant (Student's t-test with Bonferroni correction).

In terms of mentum skin stimulation, minocycline suppressed the pl-ION-induced increase of cortical responses in S1 ($0.44 \pm 0.04\%$, N = 15; $p < 0.016$; Student's t-test with Bonferroni correction). In addition, there was no significant difference in the amplitude between 3d-Sham and 3d-pl-ION + minocycline ($p = 0.18$, Student's t-test with Bonferroni correction). On the other hand, in the group of 3d-pl-ION with minocycline, excitation in S2/IOR ($0.32 \pm 0.03\%$, N = 15) had a tendency of smaller amplitude of cortical excitation to that in 3d-pl-ION ($p = 0.05$, Student's t-test with Bonferroni correction), though this amplitude was significantly larger than that in 3d-Sham ($p < 0.016$, Student's t-test with Bonferroni correction). These results suggest that minocycline suppresses pl-ION-induced facilitative neural activities, which may be a part of mechanism for inducing ectopic pain.

Effects of pl-ION and minocycline on the area of cortical excitation

Accompanied with the analysis of the amplitude of cortical excitation responding to orofacial stimulation, the area of excitation was analyzed in the Sham, pl-ION model, and minocycline-administered model. Although the excited area should be quantified by measuring the pixels whose signals exceeded the threshold, the cortical excitation frequently propagated to the dorsal S1 and S2 especially in 3d-pl-ION (Fig. 4). Therefore, the accurate quantification of the excited area could not be done in the present study. Alternatively, the areas of excitation were merged at the timing when the excitation amplitude reached the peak, and I specified the outline of the excited areas overlapped in $\geq 50\%$ animals.

In term of the stimulation of uninjured branches of maxillary and mandibular nerves, the area analysis showed the similar tendency, i.e. a facilitative effect of pl-ION and a suppressive effect of minocycline in consistent with the analysis of the amplitude (Fig. 4). In 3d-pl-ION, the excited area responding to electrical stimulation of the mandibular molar pulp and mentum skin expanded especially toward the dorsal region, which corresponds to S1 and S2. On the other hand, minocycline administration reduced the facilitative expansion of excitatory area by pl-ION (Fig. 4), which corresponded to the analysis of the amplitude of the cortical excitation.

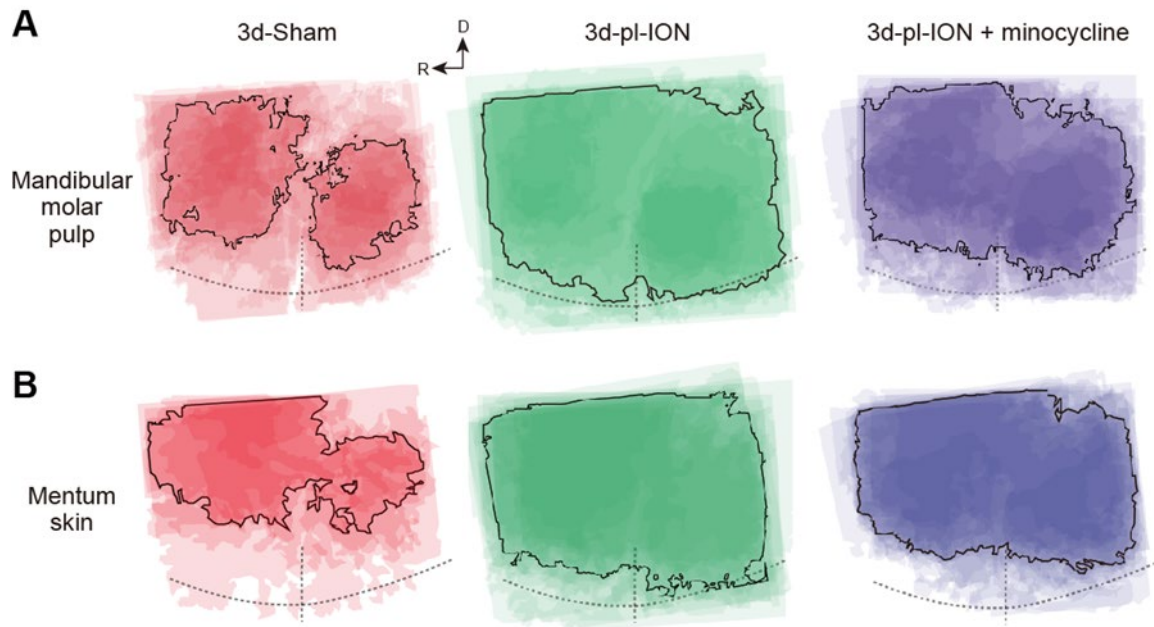


Figure 4. Spatial profile of cortical responses to electrical stimulation of the mandibular molar pulp and mentum skin. (A,B) Superimposed images of the maximum responses evoked by the mandibular molar pulp stimulation (A) and mentum skin stimulation (B) in 3d-Sham, 3d-pl-ION, and 3d-pl-ION+minocycline. R, rostral; D, dorsal.

Discussion

The present study demonstrated the neuroplastic changes in the spatiotemporal excitation patterns in S1/2 and IC of the model with pl-ION. The response to the whisker pad skin stimulation, which activates regions innervated by injured ION, was suppressed, whereas S1/2 and IC responses were facilitated to the stimulation of the mandibular molar pulp and mentum skin, which are innervated by adjacent branches of the maxillary nerve including ION. These changes are considered to underlie the ectopic pain induced by pl-ION. Administration of minocycline partially inhibited these cortical changes, suggesting that suppression of microglial activation may be effective to suppress ectopic pain induction.

Hypoexcitation in S1/S2 responding to whisker pad skin stimulation

According to the previous study, electrical stimulation of the whisker pad skin in control rats induced excitation rather in the dorsal region compared to the cortical responses to the mandibular molar pulp and mentum skin (Nakamura et al., 2015; Figs. 2-4). This area corresponds to the barrel cortex, which is clearly presented by flat mount sections (Nakamura et al., 2015). It is known that whisker sensation is processed in both S1 and S2 with the barrel structure in layer IV (Woolsey and Van der Loos, 1970), and the somatotopic map showed these fields symmetrically organized. Therefore, it is difficult to discriminate whether the excited region is located in S1 or S2 by the view of the cortical surface, and I did not discriminate between S1 and S2 excited regions in the experiment of stimulating the whisker pad stimulation. While several recordings showed a clear excitation in S2/IOI responding to whisker pad skin stimulation, most cases showed a faint activation in S2/IOI, and thus, I did

not analyzed the excitation kinetics in S2/IOF.

The treatment of pl-ION injures a part of nerve fibers of IOF, and therefore, it is reasonable that 3d-pl-ION showed lower excitation in S1/S2 responding to whisker pad stimulation. However, behavioral studies including the present study have demonstrated the hyperexcitability of neural activities in the primary and secondary neurons (Toyama et al., 2017; Zhang et al., 2017). This seems to contradict to the result of suppressive cortical excitation in 3d-pl-ION. A possible explanation for the discrepancy is that pl-ION increases spontaneous neural activities of the secondary neurons in Vc (Martin et al., 2010), and these activities may induce continuous excitation of the cortical neurons. Indeed, Latremoliere et al., (2008) reported an increase in spontaneous behaviors correlating to pain: an increment of face-grooming activity. If this is the case, the present optical imaging technique cannot estimate the increase in the baseline activities, because I quantified the differences between evoked and baseline signals as mentioned in the Materials and Methods. This discrepancy should be further explored by another method such as in vivo Ca^{2+} imaging.

Hyperexcitation in S1 and S2/IOF responding to mandibular dental pulp and mentum skin stimulation

In contrast to the responses to the whisker pad skin stimulation, mandibular molar pulp stimulation and mentum skin stimulation in pl-ION models induced larger excitatory responses in S1 and S2/IOF than those in controls. Because S1 exhibits a clear somatotopy, the expanded excitatory propagation in S1 is a possible underlying mechanism for the enlargement of the receptive field in the orofacial area and lower capacity to detect the stimulated region. In addition, larger response in S1 may contribute to hypersensitivity responding to mechanical sensation.

On the other hand, S2/IOF is likely to detect nociception rather than touch (Kobayashi and Horinuki, 2017). For example, electrical and mechanical stimuli of the periodontal ligaments induce excitation principally in S2/IOF and S1, respectively (Horinuki et al., 2015; Kaneko et al., 2017). According to this idea, larger excitation in S2/IOF may reflect higher sensitivity to nociceptive inputs, which would cause hyperalgesia and allodynia. These results are consistent with behavioral findings of the decrease in HWT reported in this and previous studies (Shinoda et al., 2007; Kubo et al., 2017).

The mechanisms for abnormal pain induced by pl-ION have been explored. Shinoda et al. (2007) demonstrated an involvement of P2X3 receptors expressed in the trigeminal ganglion neurons. Several neurochemical marker expressions including calcitonin gene-related peptide and substance P, and NK1 receptors are also changed in Vc, where the secondary neurons exist (Xu et al., 2008). In contrast, little information has been obtained with respect to the contribution of higher brain regions to abnormal pain induced by pl-ION. I consider that not only the primary and secondary neurons but also the cerebrocortical neurons and their local

circuits may be changed by pl-ION, because the transection model of the inferior alveolar nerve shows hyperexcitation, which accompanies neuroplastic changes in excitatory and inhibitory synaptic transmission in the cortical circuits (Fujita et al., 2019).

Minocycline relieves trigeminal neuropathic pain

Minocycline is a popular tetracycline, which inhibits protein synthesis of bacteria by a blockade of tRNA binding to ribosomal subunit (30S). In the nervous system, minocycline is known to inhibit activation of microglia, and cytokines and other bioactive substances have been reported to be involved in modulation of microglial activities: interleukin (IL)-1, IL-1 β , IL-6, nitric oxide, prostaglandin, and so on (Yrjanheikki et al., 1999; Stirling et al., 2005; Latremoliere et al., 2008).

It has been explored whether minocycline administration relieves neuropathic pain that occurs in the orofacial regions innervated by the trigeminal nerve (Piao et al., 2006; Latremoliere et al., 2008; Shibuta et al., 2012). The inferior alveolar nerve and mental nerve transection model that shows hypersensitivity estimated by mechanical stimulation of the whisker pad show minocycline-dependent suppression of hypersensitivity possibly by inhibiting p38 mitogen-activated protein kinase in microglia of Vc (Piao et al., 2006). Shibuta et al. (2012) demonstrated that minocycline suppresses activation of microglia in parallel to the attenuation of Vc neuronal activities in the pl-ION model showing mechanical allodynia. The present results that minocycline partially recovers cortical activity changes induced by pl-ION corroborate these previous reports.

I consider that inhibition of microglial activation before pl-ION is critical in minocycline-induced recovery of cortical response changes by pl-ION. The pilot study suggests that the effect of minocycline application started just after ION and sequential application once a day (1 mg/kg) had little effect on cortical responses. This issue should be further examined in the future.

Conclusions

Optical imaging that enables us to visualize spatiotemporal excitation *in vivo* preparation was conducted to elucidate how somatosensory information of peripheral organs innervated by the maxillary nerve are processed in the cerebral cortex. First, anatomical relationship, i.e. somatotopic organization, between the nasal mucosa and surrounding regions and cerebral cortex was clarified: somatosensation induced by air puff application to the nasal mucosa and skin, and upper pharynx are processed in spatially continuous regions of S1, and interaction between somatosensory and these regions receives little olfactory information. Second, the pathophysiological profile of the cerebral cortex responding to pl-ION was elucidated. Cerebral cortical responses to the mandibular molar dental pulp and mentum skin stimuli increased both in S1 and S2/IOR after pl-ION, which was partially recovered by administration of minocycline from 1 d before to 2 d after pl-ION. These characterized features of cortical responses may contribute to develop a new pharmacotherapy for trigeminal abnormal pain.

Acknowledgements

I am grateful to Prof. Morio Tonogi for the opportunity to perform this study, Prof. Masayuki Kobayashi for supervising this study, and colleagues in Department of Pharmacology for their technical advice and assistance.

References

- Albrecht J, Kopietz R, Frasnelli J, Wiesmann M, Hummel T, Lundström JN (2010) The neuronal correlates of intranasal trigeminal function-an ALE meta-analysis of human functional brain imaging data. *Brain Res Rev* 62: 183-196.
- Allen GV, Saper CB, Hurley KM, Cechetto DF (1991) Organization of visceral and limbic connections in the insular cortex of the rat. *J Comp Neurol* 311: 1-16.
- Anton F, Peppel P (1991) Central projections of trigeminal primary afferents innervating the nasal mucosa: a horseradish peroxidase study in the rat. *Neuroscience* 41: 617-628.
- Benison AM, Rector DM, Barth DS (2007) Hemispheric mapping of secondary somatosensory cortex in the rat. *J Neurophysiol* 97: 200-207.
- Berger T, Borgdorff A, Crochet S, Neubauer FB, Lefort S, Fauvet B, Ferezou I, Carleton A, Lüscher HR, Petersen CC (2007) Combined voltage and calcium epifluorescence imaging in vitro and in vivo reveals subthreshold and suprathreshold dynamics of mouse barrel cortex. *J Neurophysiol* 97: 3751-3762.
- Bojsen-Møller F (1975) Demonstration of terminalis, olfactory, trigeminal and perivascular nerves in the rat nasal septum. *J Comp Neurol* 159: 245-256.
- Brand G (2006) Olfactory/trigeminal interactions in nasal chemoreception. *Neurosci Biobehav Rev* 30: 908-917.
- Civillico EF, Contreras D (2005) Comparison of responses to electrical stimulation and whisker deflection using two different voltage-sensitive dyes in mouse barrel cortex in vivo. *J Membr Biol* 208: 171-182.
- Croy I, Schulz M, Blumrich A, Hummel C, Gerber J, Hummel T (2014) Human olfactory lateralization requires trigeminal activation. *Neuroimage* 98: 289-295.
- Enomoto K, Takahashi R, Katada A, Nonaka S (1998) The augmentation of intrinsic laryngeal muscle activity by air-jet stimulation of the nasal cavity in decerebrate cats. *Neurosci Res* 31: 137-146.
- Fujita S, Adachi K, Koshikawa N, Kobayashi M (2010) Spatiotemporal dynamics of excitation in rat insular cortex: intrinsic corticocortical circuit regulates caudal-rostral excitatory propagation from the insular to frontal cortex. *Neuroscience* 165: 278-292.
- Fujita S, Kitayama T, Mizoguchi N, Oi Y, Koshikawa N, Kobayashi M (2012) Spatiotemporal profiles of transcallosal connections in rat insular cortex revealed by *in vivo* optical imaging. *Neuroscience* 206: 201-211.
- Fujita S, Mizoguchi N, Aoki R, Cui Y, Koshikawa N, Kobayashi M (2016) Cytoarchitecture-dependent decrease in propagation velocity of cortical spreading depression in the rat insular cortex revealed by optical imaging. *Cereb Cortex* 26:1580-1589.
- Fujita S, Kaneko M, Nakamura H, Kobayashi M (2017) Spatiotemporal profiles of proprioception processed by the masseter muscle spindles in rat cerebral cortex: an optical imaging study. *Front Neural Circuits* 11: 4.

- Fujita S, Yamamoto K, Kobayashi M (2019) Trigeminal nerve transection-induced neuroplastic changes in the somatosensory and insular cortices in a rat ectopic pain model. *eNeuro* 6.
- Gastl M, Br  nner YF, Wiesmann M, Freiherr J (2014) Depicting the inner and outer nose: the representation of the nose and the nasal mucosa on the human primary somatosensory cortex (SI). *Hum Brain Mapp* 35: 4751-4766.
- Horinuki E, Shinoda M, Shimizu N, Koshikawa N, Kobayashi M (2015) Orthodontic force facilitates cortical responses to periodontal stimulation. *J Dent Res* 94: 1158-1166.
- Horinuki E, Yamamoto K, Shimizu N, Koshikawa N, Kobayashi M (2016) Sequential changes in cortical excitation during orthodontic treatment. *J Dent Res* 95: 897-905.
- Johnson BA, Leon M (2007) Chemotopic odorant coding in a mammalian olfactory system. *J Comp Neurol* 503: 1-34.
- Kaneko M, Fujita S, Shimizu N, Motoyoshi M, Kobayashi M (2018) Experimental tooth movement temporally changes neural excitation and topographical map in rat somatosensory cortex. *Brain Res* 1698: 62-69.
- Kaneko M, Horinuki E, Shimizu N, Kobayashi M (2017) Physiological profiles of cortical responses to mechanical stimulation of the tooth in the rat: An optical imaging study. *Neuroscience* 358: 170-180.
- Kobayashi M, Fujita S, Takei H, Song L, Chen S, Suzuki I, Yoshida A, Iwata K, Koshikawa N (2010) Functional mapping of gustatory neurons in the insular cortex revealed by pERK-immunohistochemistry and in vivo optical imaging. *Synapse* 64: 323-334.
- Kobayashi M, Horinuki E (2017) Neural mechanisms of nociception during orthodontic treatment. *J Oral Sci* 59: 167-171.
- Kubo A, Shinoda M, Katagiri A, Takeda M, Suzuki T, Asaka J, Yeomans DC, Iwata, K (2017) Oxytocin alleviates orofacial mechanical hypersensitivity associated with infraorbital nerve injury through vasopressin-1A receptors of the rat trigeminal ganglia. *Pain* 158: 649-659.
- Latremoliere A, Mauborgne A, Masson J, Bourgoin S, Kayser V, Hamon M, Pohl M (2008) Differential implication of proinflammatory cytokine interleukin-6 in the development of cephalic versus extracephalic neuropathic pain in rats. *J Neurosci* 28: 8489-8501.
- Lippert MT, Takagaki K, Xu W, Huang X, Wu JY (2007) Methods for voltage-sensitive dye imaging of rat cortical activity with high signal-to-noise ratio. *J Neurophysiol* 98: 502-512.
- Martin YB, Malmierca E, Avendano C, Nunez A (2010) Neuronal disinhibition in the trigeminal nucleus caudalis in a model of chronic neuropathic pain. *Eur J Neurosci* 32: 399-408.
- Mitchell JL, Silverman MB, Aicher SA (2004) Rat trigeminal lamina I neurons that project to thalamic or parabrachial nuclei contain the mu-opioid receptor. *Neuroscience* 128: 571-582.
- Nakamura H, Kato R, Shirakawa T, Koshikawa N, Kobayashi M (2015) Spatiotemporal profiles of dental pulp nociception in rat cerebral cortex: an optical imaging study. *J Comp*

- Neurol 523: 1162-1174.
- Nakamura H, Shirakawa T, Koshikawa N, Kobayashi M (2016) Distinct excitation to pulpal stimuli between somatosensory and insular cortices. *J Dent Res* 95: 180-187.
- Paxinos G, Watson C (2007) The rat brain in stereotaxic coordinates, 6th ed. New York: Academic Press.
- Piao ZG, Cho IH, Park CK, Hong JP, Choi SY, Lee SJ, Lee S, Park K, Kim JS, Oh SB (2006) Activation of glia and microglial p38 MAPK in medullary dorsal horn contributes to tactile hypersensitivity following trigeminal sensory nerve injury. *Pain* 121: 219-231.
- Qiu S, Chen T, Koga K, Guo YY, Xu H, Song Q, Wang JJ, Descalzi G, Kaang BK, Luo JH, Zhuo M, Zhao MG (2013) An increase in synaptic NMDA receptors in the insular cortex contributes to neuropathic pain. *Sci Signal* 6: ra34.
- Remple MS, Henry EC, Catania KC (2003) Organization of somatosensory cortex in the laboratory rat (*Rattus norvegicus*): Evidence for two lateral areas joined at the representation of the teeth. *J Comp Neurol* 467: 105-118.
- Rennaker RL, Chen CF, Ruyle AM, Sloan AM, Wilson DA (2007) Spatial and temporal distribution of odorant-evoked activity in the piriform cortex. *J Neurosci* 27:1534-1542.
- Sant'Ambrogio G, Tsubone H, Sant'Ambrogio FB (1995) Sensory information from the upper airway: role in the control of breathing. *Respir Physiol* 102: 1-16.
- Sato T, Hirono J, Hamana H, Ishikawa T, Shimizu A, Takashima I, Kajiwarara R, Iijima T (2008) Architecture of odor information processing in the olfactory system. *Anat Sci Int* 83: 195-206.
- Sekizawa SI, Ishikawa T, Sant'Ambrogio G (1998) Asymmetry in reflex responses of nasal muscles in anesthetized guinea pigs. *J Appl Physiol* 85: 123-128.
- Shi CJ, Cassell MD (1998) Cascade projections from somatosensory cortex to the rat basolateral amygdala via the parietal insular cortex. *J Comp Neurol* 399: 469-491.
- Shibuta K, Suzuki I, Shinoda M, Tsuboi Y, Honda K, Shimizu N, Sessle BJ, Iwata K (2012) Organization of hyperactive microglial cells in trigeminal spinal subnucleus caudalis and upper cervical spinal cord associated with orofacial neuropathic pain. *Brain Res* 1451: 74-86.
- Shinoda M, Kawashima K, Ozaki N, Asai H, Nagamine K, Sugiura Y (2007) P2X₃ receptor mediates heat hyperalgesia in a rat model of trigeminal neuropathic pain. *J Pain* 8: 588-597.
- Stettler DD, Axel R (2009) Representations of odor in the piriform cortex. *Neuron* 63: 854-864.
- Stirling DP, Koochesfahani KM, Steeves JD, Tetzlaff W (2005) Minocycline as a neuroprotective agent. *Neuroscientist* 11: 308-322.
- Takemura M, Sugiyo S, Moritani M, Kobayashi M, Yonehara N (2006) Mechanisms of orofacial pain control in the central nervous system. *Arch Histol Cytol* 69: 79-100.
- Taylor AM, Ribeiro-Da-Silva A (2011) GDNF levels in the lower lip skin in a rat model of trigeminal neuropathic pain: implications for nonpeptidergic fiber reinnervation and

- parasympathetic sprouting. *Pain* 152: 1502-1510.
- Toyama M, Kudo C, Mukai C, Inoue M, Oyamaguchi A, Hanamoto H, Sugimura M, Niwa H (2017) Trigeminal nervous system sensitization by infraorbital nerve injury enhances responses in a migraine model. *Cephalalgia* 37: 1317-1328.
- Tsubone H (1989) Nasal 'flow' receptors of the rat. *Respir Physiol* 75: 51-64.
- Tsubone H (1990) Nasal 'pressure' receptors. *Jpn J Vet Sci* 52: 225-232.
- Vos BP, Strassman AM, Maciewicz RJ (1994) Behavioral evidence of trigeminal neuropathic pain following chronic constriction injury to the rat's infraorbital nerve. *J Neurosci* 14: 2708-2723.
- Waite PM, Taylor PK (1978) Removal of whiskers in young rats causes functional changes in cerebral cortex. *Nature* 274: 600-602.
- Woolsey TA, Van Der Loos H (1970) The structural organization of layer IV in the somatosensory region (SI) of mouse cerebral cortex. The description of a cortical field composed of discrete cytoarchitectonic units. *Brain Res* 17: 205-242.
- Xu M, Aita M, Chavkin C (2008) Partial infraorbital nerve ligation as a model of trigeminal nerve injury in the mouse: behavioral, neural, and glial reactions. *J Pain* 9: 1036-1048.
- Yrjanheikki J, Tikka T, Keinanen R, Goldsteins G, Chan PH, Koistinaho J (1999) A tetracycline derivative, minocycline, reduces inflammation and protects against focal cerebral ischemia with a wide therapeutic window. *Proc Natl Acad Sci USA* 96: 13496-13500.
- Yu X, Wang S, Chen DY, Dodd S, Goloshevsky A, Koretsky AP (2010) 3D mapping of somatotopic reorganization with small animal functional MRI. *Neuroimage* 49: 1667-1676.
- Zama M, Hara Y, Fujita S, Kaneko T, Kobayashi M (2018) Somatotopic organization and temporal characteristics of cerebrocortical excitation in response to nasal mucosa stimulation with and without an odor in the Rat: An optical imaging study. *Neuroscience* 377: 77-86.
- Zhang Q, Zhu MD, Cao DL, Bai XQ, Gao YJ, Wu XB (2017) Chemokine CXCL13 activates p38 MAPK in the trigeminal ganglion after infraorbital nerve injury. *Inflammation* 40: 762-769.